Electronic Supplementary Material (ESI) for Journal of Materials Chemistry A.

Supporting Information

Surface-Mounted MOF Thin Film with Oriented Nanosheet Arrays for Enhancing Oxygen Evolution Reaction

De-Jing Li,[ab§] Qiao-Hong Li,[a§] Zhi-Gang Gu[a] and Jian Zhang[a]*

[a] State Key Laboratory of Structural Chemistry, Fujian Institute of Research on the Structure of Matter, Chinese Academy of Sciences, Fuzhou, Fujian 350002, P. R. China

[b] University of Chinese Academy of Sciences, Beijing 100049, P.R. China

[§] These authors contributed equally to this work

E-mail: zggu@fjirsm.ac.cn

Table of content

powder deposited on Cu foam; (c) The LSV curves of Co/Ni$(BDC)_2$TED deposited on Cu foam and Co/Ni$(BDC)_2$TED@CF; (d) Chronopotentiometric curves of Co/Ni$(BDC)_2$TED deposited on Cu foam and Co/Ni$(BDC)_2$TED@CF.

Figure S15. Faradaic efficiency for Co/Ni$(BDC)_2$TED@CF at the current density of 50 mA cm^{-2}.

Figure S16. (a) CV of Co/Ni$(BDC)_2$TED@CF at different scan rates of 5, 10, 15, 20, and 25 mV s^{-1} in 1.0 M KOH and (b) the linear relationship of the oxidation peak currents vs. scan rates for theCo/Ni$(BDC)_2$TED@CF.

Figure S17. (a) CV of $Ni_2(BDC)_2$TED@CF at different scan rates of 5, 10, 15, 20, and 25 mV s^{-1} in 1.0 M KOH and (b) the linear relationship of the oxidation peak currents vs. scan rates for the $Ni_2(BDC)_2$TED@CF.

Figure S18. (a) CV of $Co_2(BDC)_2$TED@CF at different scan rates of 5, 10, 15, 20, and 25 mV s^{-1} in 1.0 M KOH and (b) the linear relationship of the oxidation peak currents vs. scan rates for the $Co_2(BDC)_2$TED@CF.

Figure S19. The SEM images after the electrochemical testing at 50 mA cm^{-2} for 10000s: (a) $Co_2(BDC)_2$TED@CF; (b) $Ni_2(BDC)_2$TED@CF; (c) Co/Ni$(BDC)_2$TED@CF; (d) The TEM images of Co/Ni$(BDC)_2$TED@CF after the electrochemical testing at 50 mA cm^{-2} for 10000 s.

Figure S20. (a) The XRD and (b) IR of Co/Ni$(BDC)_2$TED@CF after the electrochemical testing.

Figure S21. The XPS results of Co/Ni$(BDC)_2$TED@CF after OER cycling.

Table S1. Comparison of Electrocatalytic Performances of Various Materials.

Figure S22. The surface SEM images of Co/Ni$(BDC)_2$TED@CF with different cycles: (a, b) 5 cycles; (c, d) 10 cycles; (e, f) 20 cycles; (g, h) 30 cycles; (i, j) 40 cycles; (k, l) 50 cycles.

Figure S23. The cross-sectional SEM images of Co/Ni$(BDC)_2$TED@CF with different cycles: (a) (b) 5 cycles; (c) (d) 10 cycles; (e) (f) 20 cycles; (g) (h) 30 cycles; (i) (j) 40 cycles; (k) (l) 50 cycles.

Figure S24. The curves of the thickness versus preparation cycles.

Figure S25. CVs of Co/Ni$(BDC)_2$TED@CF with different thickness at the different scan rates

from 10-100 mV s^{-1} in the potential range of 0.01-0.1 V vs Ag/AgCl: (a) 5 cycles; (b) 10 cycles; (c) 20 cycles; (d) 30 cycles; (e) 40 cycles; (f) 50 cycles.
Figure S26. Capacitive current at 0.06 V vs Ag/AgCl for Co/Ni$(BDC)_2$TED@CF with different thickness.
Figure S27. The ECSA normalized LSV curves of Co/Ni$(BDC)_2$TED@CF with different thickness.
Figure S28. The SEM EDS date of Co/Ni$(BDC)_2$TED@CF with a Co/Ni ratio of 1/1.5(Cu is from Cu foam).
Figure S29. The SEM EDS date of Co/Ni$(BDC)_2$TED@CF with a Co/Ni ratios of 1/0.5(Cu is from Cu foam).
Figure S30. The SEM EDS date of Co/Ni$(BDC)_2$TED@CF with a Co/Ni ratios of 1/1(Cu is from Cu foam).
Figure S31. The SEM mapping in Co/Ni$(BDC)_2$TED@CF with a Co/Ni ratios of 1/1.5.
Figure S32. The SEM mapping in Co/Ni$(BDC)_2$TED@CF with a Co/Ni ratios of 1/0.5.
Figure S33. The SEM mapping in Co/Ni$(BDC)_2$TED@CF with a Co/Ni ratios of 1/1.
Figure S34. (a) The polarization curves for Co/Ni$(BDC)_2$TED@CF with different Co/Ni ratios; (b) The overpotential of Co/Ni$(BDC)_2$TED@CF with different Co/Ni ratios at the current density of 50 mA cm^{-2}; (c) The EIS curves; (d) The Tafel plots from the LSV curves.
Figure S35. CVs of Co/Ni$(BDC)_2$TED@CF with different Co/Ni ratios at the different scan rates from 10-100 mV s^{-1} in the potential range of 0.01-0.1 V vs Ag/AgCl: (a) Co/Ni(1/05); (b) Co/Ni(1/1); (c) Co/Ni(1/1.5) and (d) Capacitive current at 0.06 V vs Ag/AgCl.
Table S2. The ICP dates of Co/Ni ratios in Co/Ni$(BDC)_2$TED@CF with different Co/Ni ratios.
Figure S36. The DFT calculation model of OER process on metal sites in the structure of $Co_2(BDC)_2$TED with [001] orientation.
Figure S37. The DFT calculation model of OER process on metal sites in the structure of

$Ni_2(BDC)_2TED$ with [001] orientation.
Figure S38. The diagrammatic graph of OER process in $Co/Ni(BDC)_2TED$ nanosheets.
Figure S39. The Gibbs free energy changes of $Co/Ni(BDC)_2TED$ nanosheets with two different models.

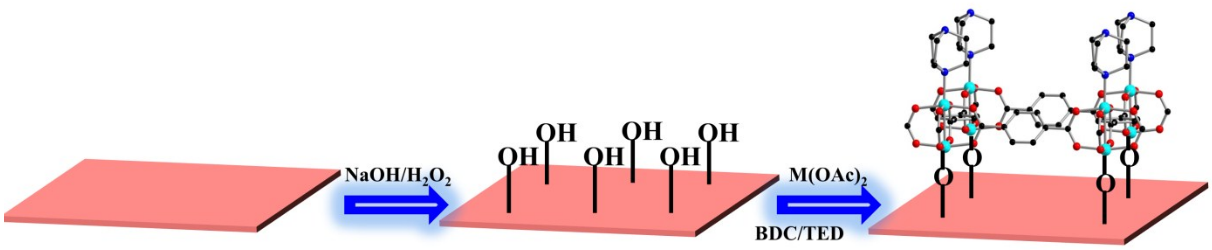

Scheme S1. Schematic illustration of the formation of $M_2(BDC)_2TED$ on the substrate.

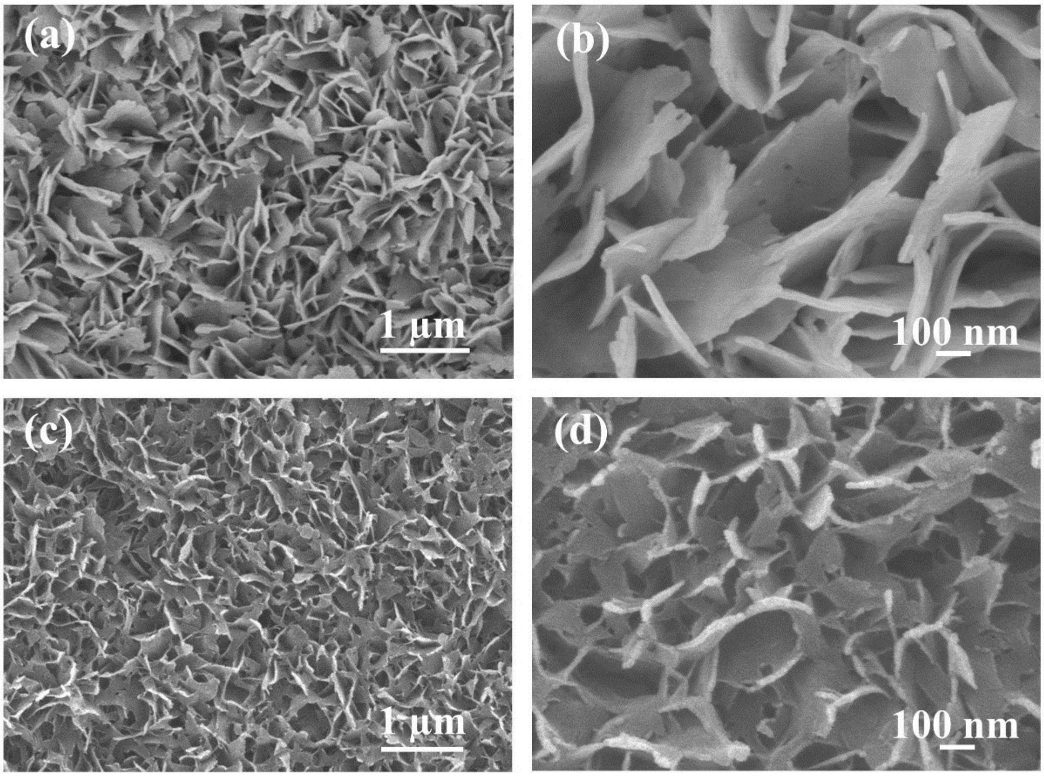

Figure S1. The surface SEM images of $M_2(BDC)_2TED$ MOF grown on the Cu foil: (a) (b) $Co_2(BDC)_2TED$; (c) (d) $Ni_2(BDC)_2TED$.

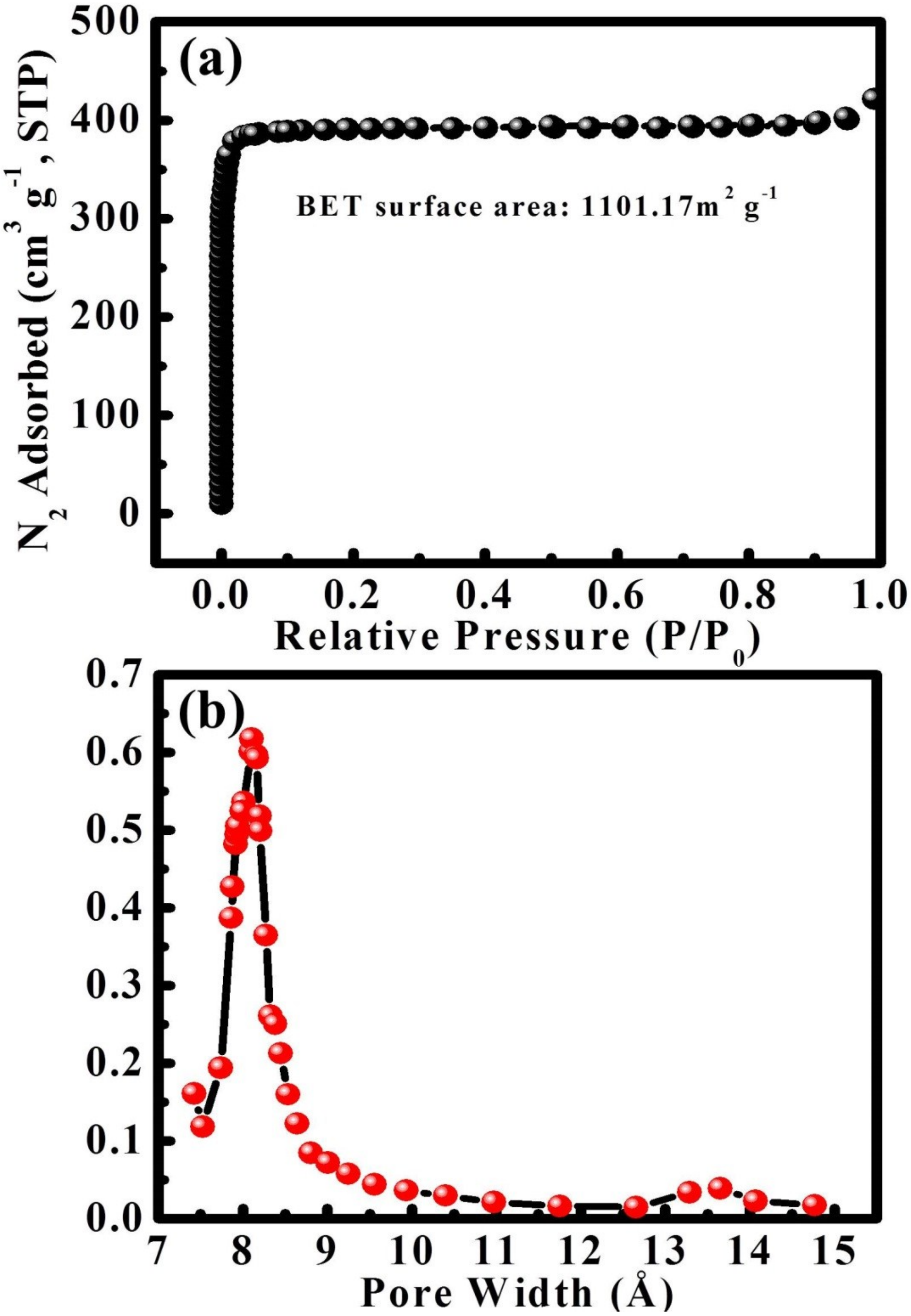

Figure S2. (a) N_2 adsorption isotherm and (b) pore size distribution of Co/Ni(BDC)$_2$TED nanosheets stripped from Cu foam.

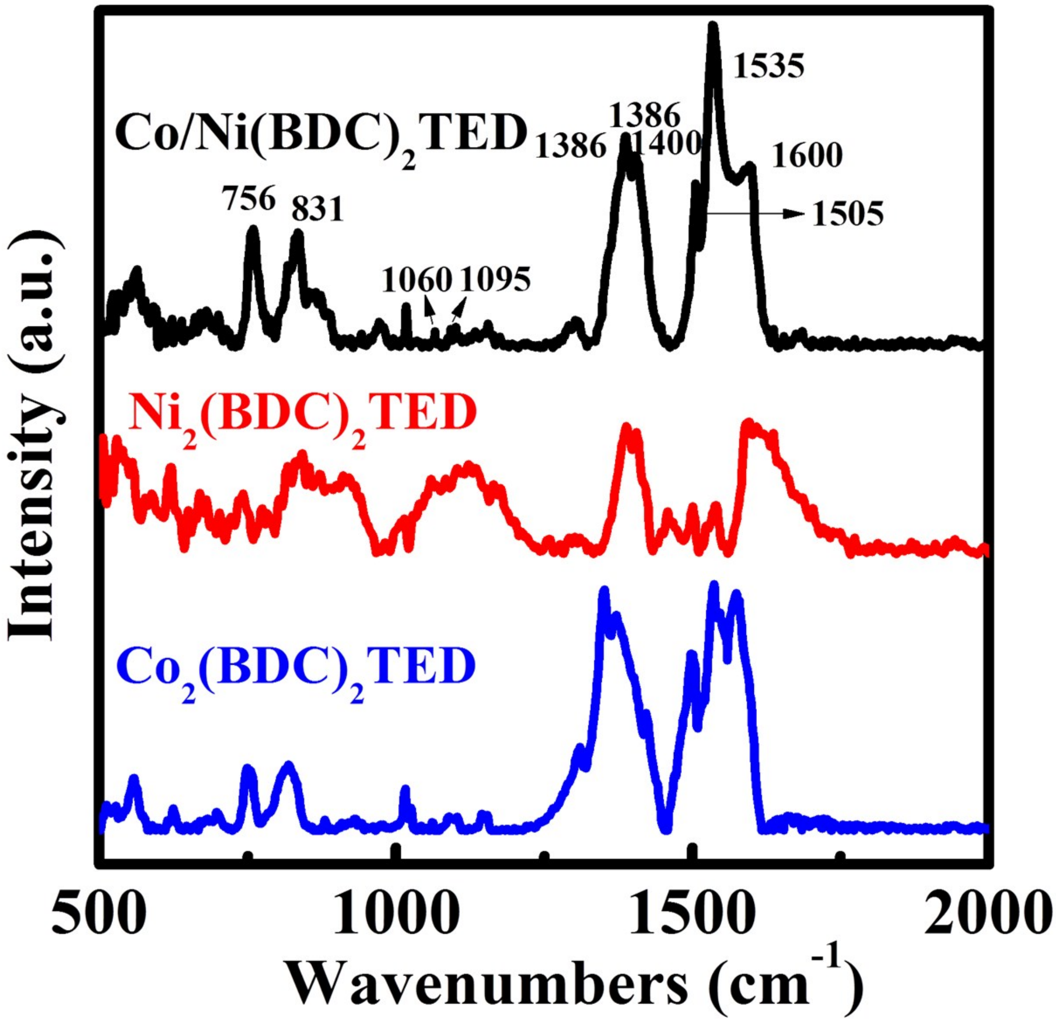

Figure S3. The IR spectrum of $Co_2(BDC)_2TED$, $Ni_2(BDC)_2TED$ and $Co/Ni(BDC)_2TED$ nanosheets stripped from Cu foam.

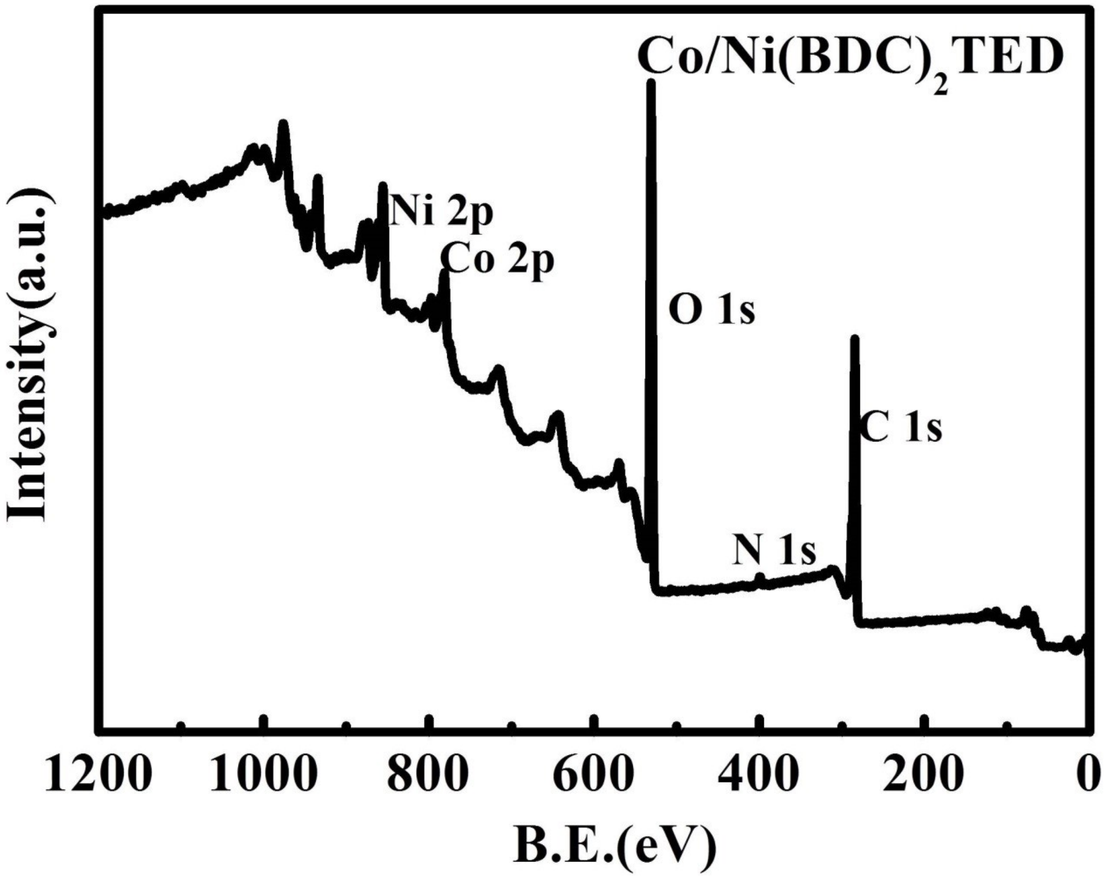

Figure S4. The XPS survey of Co/Ni(BDC)$_2$TED@CF.

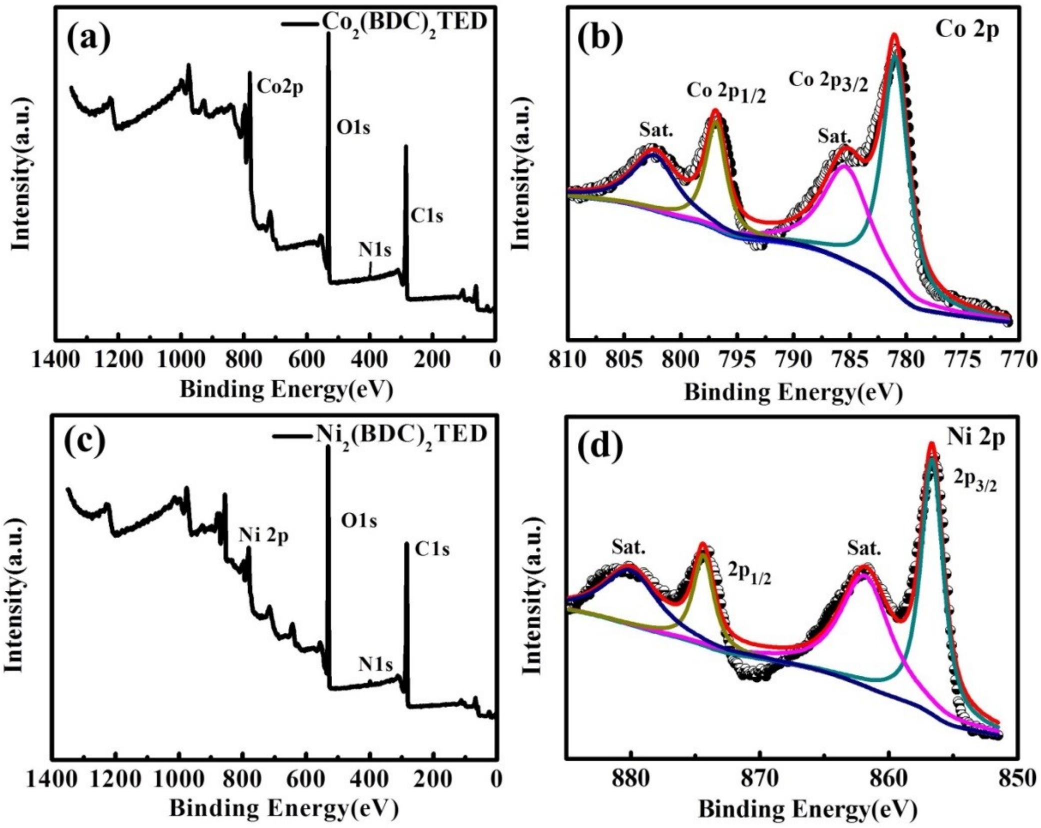

Figure S5. The XPS results: (a) (b) $Co_2(BDC)_2TED$@CF; (c) (d) $Ni_2(BDC)_2TED$@CF.

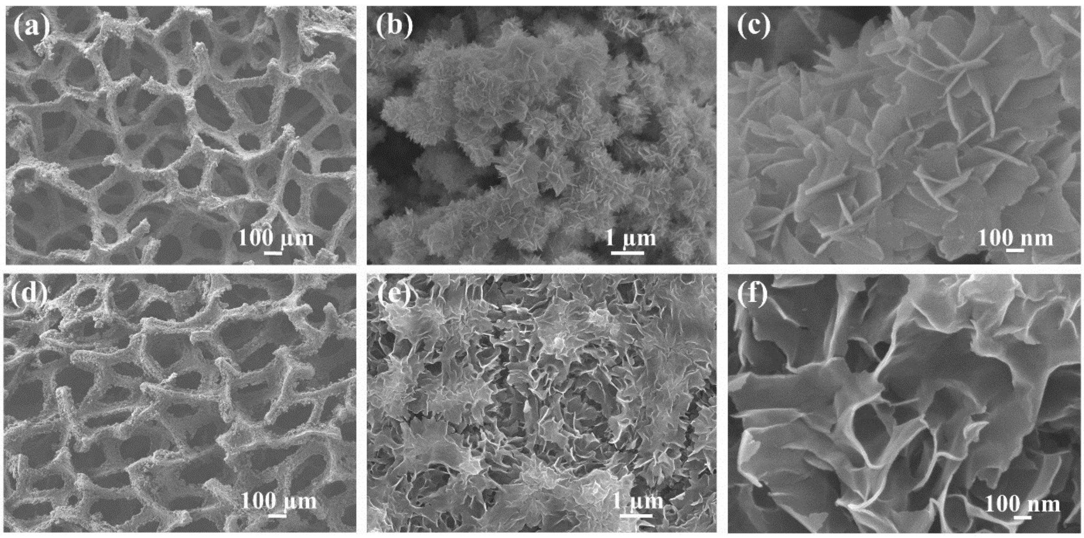

Figure S6. The surface SEM images of $M_2(BDC)_2TED$ MOF grown on the Cu foam: (a, b, c) $Co_2(BDC)_2TED$@CF; (d, e, f) $Ni_2(BDC)_2TED$@CF.

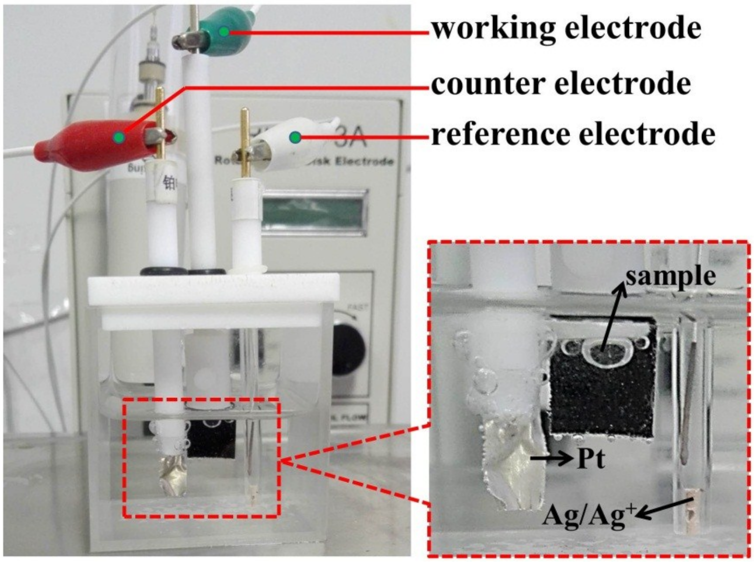

Figure S7. The setup of electrochemical measurement.

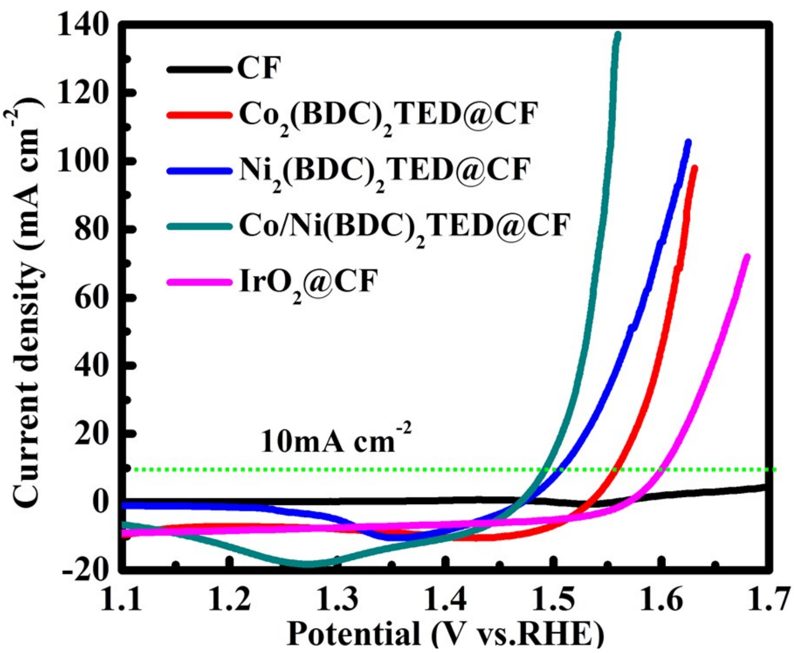

Figure S8. LSV curves in the reverse sweep direction.

The presence of strong oxidation peaks of Ni^{2+} to Ni^{3+} in LSV curves of the catalysis (Figure 3a), so we can obtain the overpotentials at the current density of 10 mA cm^{-2} in the LSV curves by the reverse sweep direction. As shown in Figure S8, Co/Ni$(BDC)_2$TED@CF requied the lowest overpotential of only 260 mV to reach the current density of 10 mA cm^{-2} , while the overpotentials of about 276, 327 and 380 mV were required to reach the current density of 10 mA cm^{-2} for $Ni_2(BDC)_2$TED@CF, $Co_2(BDC)_2$TED@CF and IrO_2@CF @CF , respectively. This order is consistent with those at the current density of 50 mA cm^{-2}, indicating the excellent OER activity of Co/Ni$(BDC)_2$TED@CF.

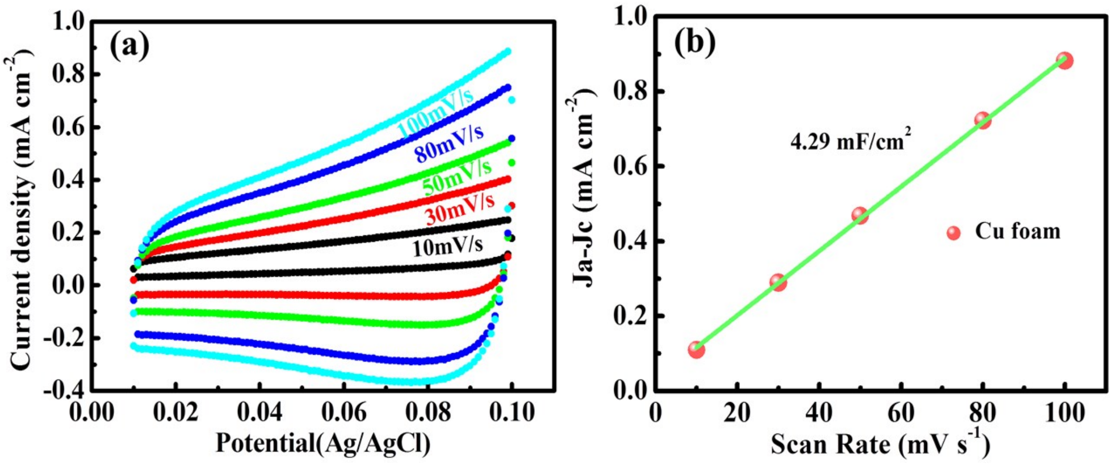

Figure S9. (a) CVs of bare Cu foam at the different scan rates from 10-100 mV s^{-1} in the potential range of 0.01-0.1 V vs Ag/AgCl and (b) Capacitive current at 0.06 V vs Ag/AgCl.

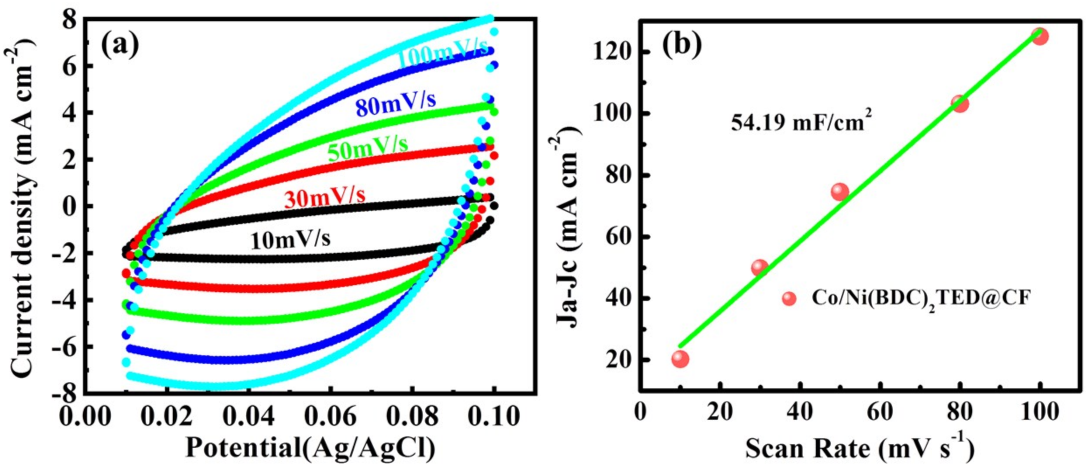

Figure S10. (a) CVs of Co/Ni $(BDC)_2TED$@CF at the different scan rates from 10-100 mV s^{-1} in the potential range of 0.01-0.1 V vs Ag/AgCl and (b) Capacitive current at 0.06 V vs Ag/AgCl.

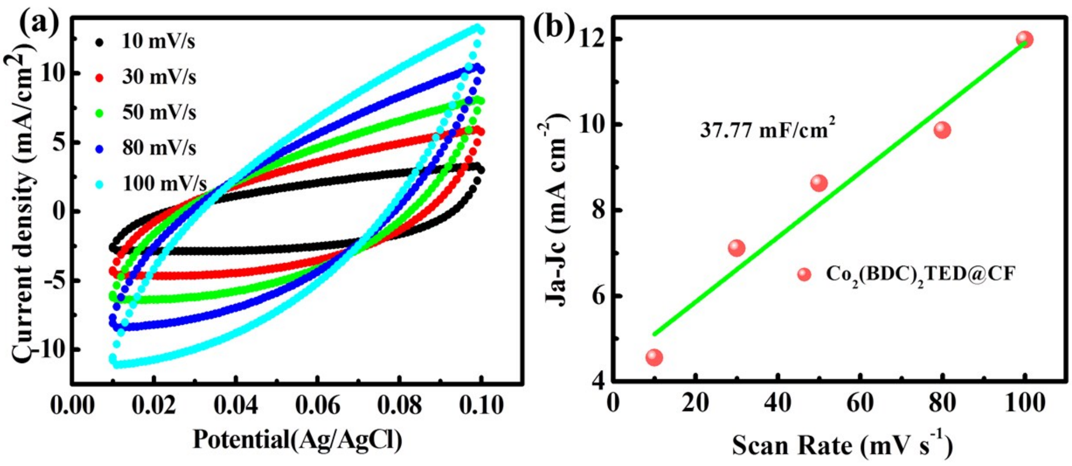

Figure S11. (a) CVs of $Co_2(BDC)_2TED$@CF at the different scan rates from 10-100 mV s^{-1} in the potential range of 0.01-0.1 V vs Ag/AgCl and (b) Capacitive current at 0.06 V vs Ag/AgCl.

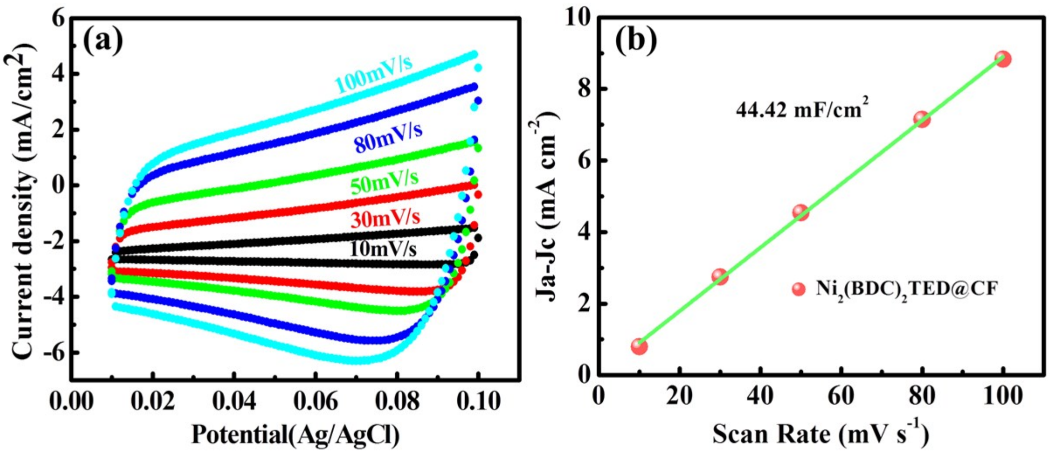

Figure S12. (a) CVs of $Ni_2(BDC)_2TED@CF$ at the different scan rates from 10-100 mV s^{-1} in the potential range of 0.01-0.1 V vs Ag/AgCl and (b) Capacitive current at 0.06 V vs Ag/AgCl.

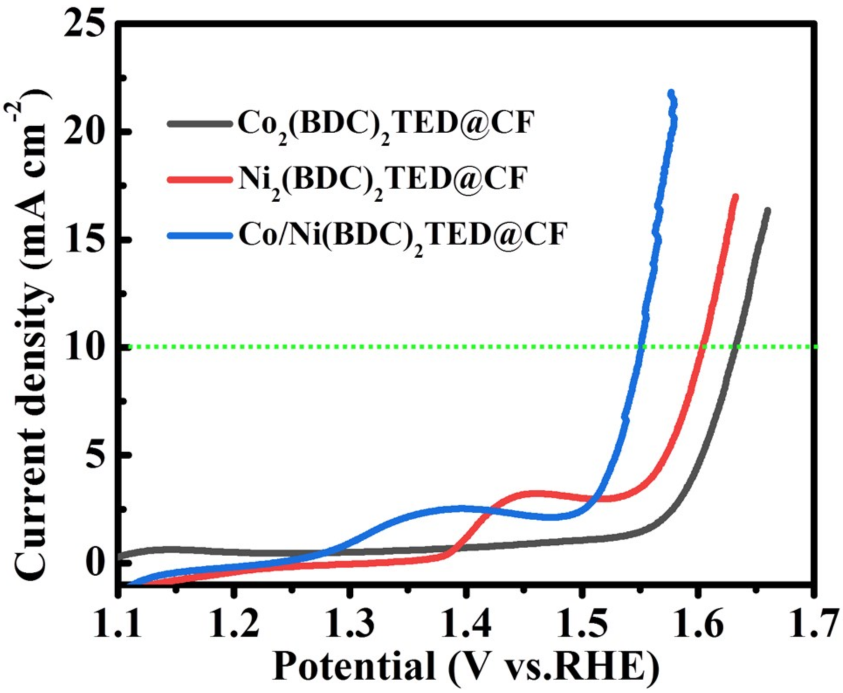

Figure S13. The ECSA normalized LSV curves.

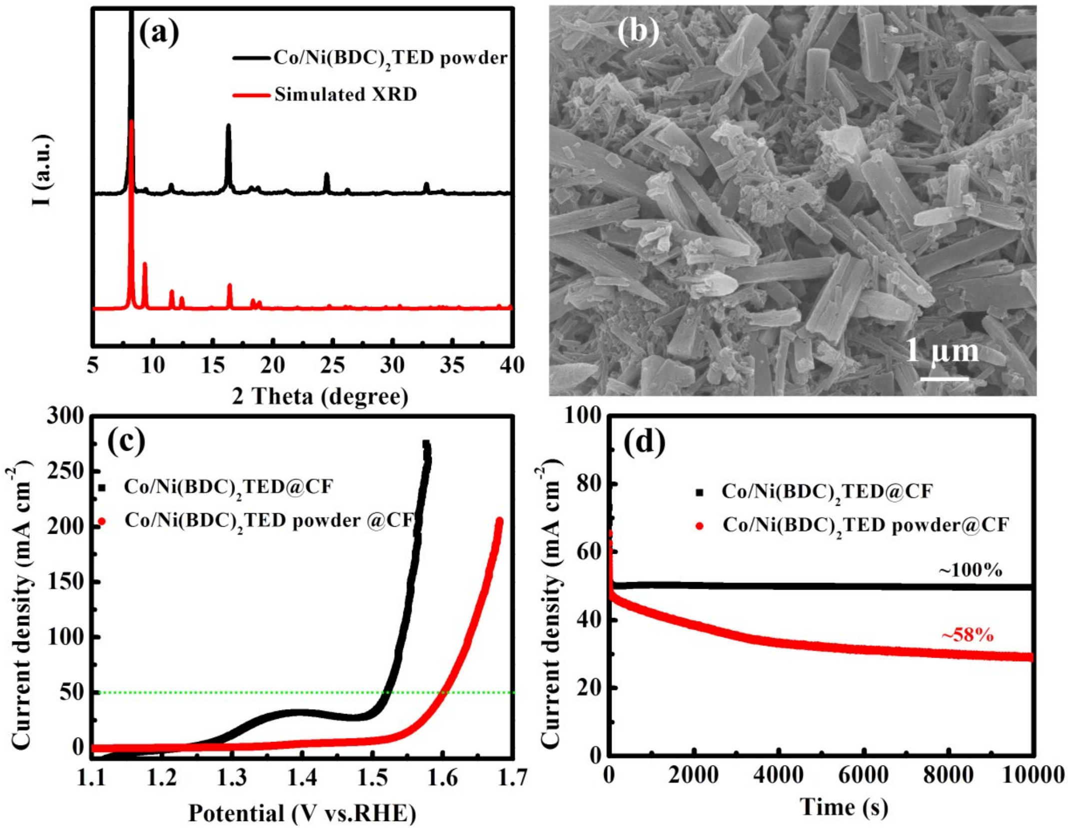

Figure S14. (a) The XRD of Co/Ni$(BDC)_2$TED powder; (b) The SEM image of Co/Ni$(BDC)_2$TED powder deposited on Cu foam; (c) The LSV curves of Co/Ni$(BDC)_2$TED deposited on Cu foam and Co/Ni$(BDC)_2$TED@CF; (d) Chronopotentiometric curves of Co/Ni$(BDC)_2$TED deposited on Cu foam and Co/Ni$(BDC)_2$TED@CF.

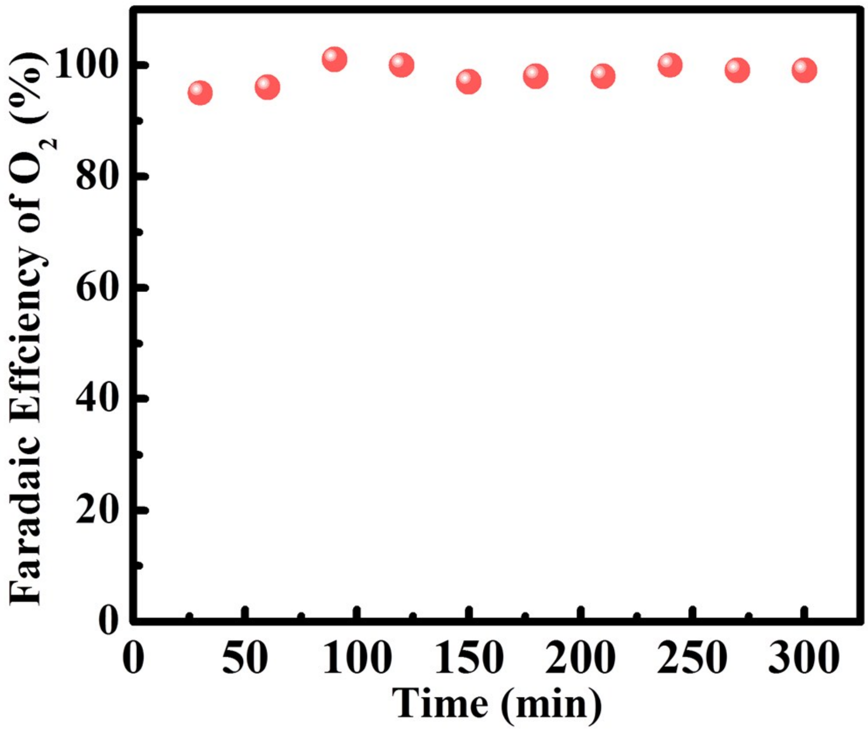

Figure S15. Faradaic efficiency for Co/Ni(BDC)$_2$TED@CF at the current density of 50 mA cm^{-2}.

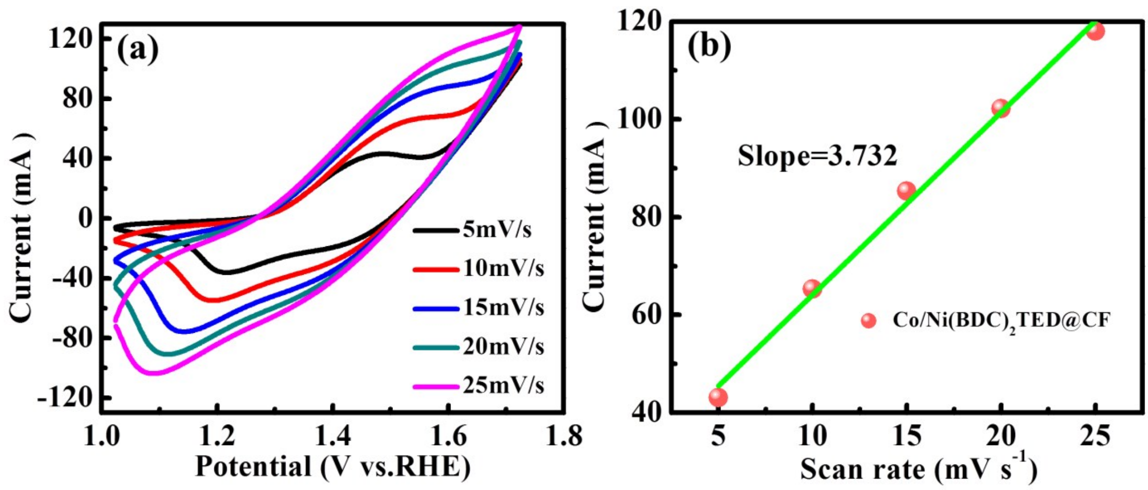

Figure S16. (a) CV of Co/Ni(BDC)$_2$TED@CF at different scan rates of 5, 10, 15, 20, and 25 mV s^{-1} in 1.0 M KOH and (b) the linear relationship of the oxidation peak currents vs. scan rates for theCo/Ni(BDC)$_2$TED@CF.

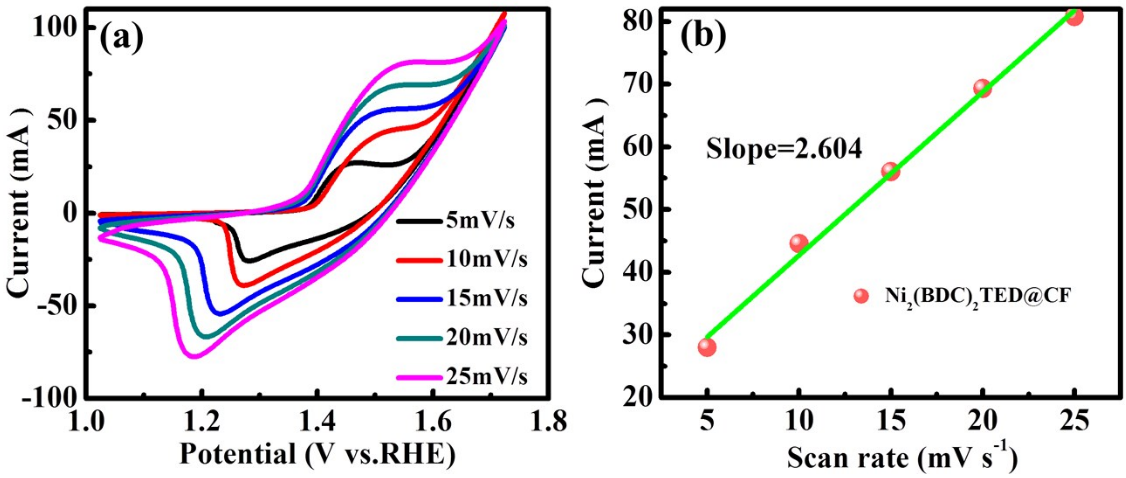

Figure S17. (a) CV of $Ni_2(BDC)_2TED@CF$ at different scan rates of 5, 10, 15, 20, and 25 mV s^{-1} in 1.0 M KOH and (b) the linear relationship of the oxidation peak currents vs. scan rates for the $Ni_2(BDC)_2TED@CF$.

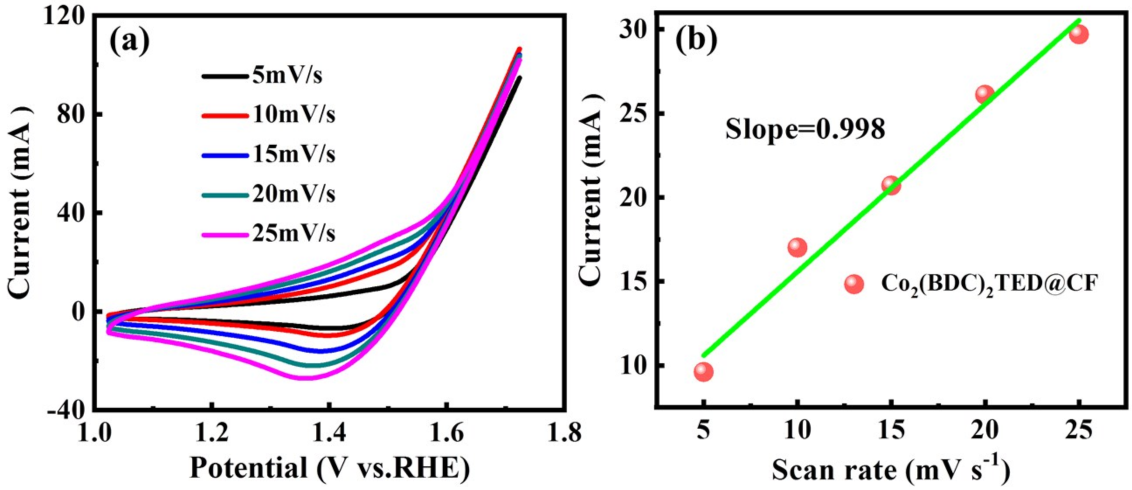

Figure S18. (a) CV of $Co_2(BDC)_2TED@CF$ at different scan rates of 5, 10, 15, 20, and 25 mV s^{-1} in 1.0 M KOH and (b) the linear relationship of the oxidation peak currents vs. scan rates for the $Co_2(BDC)_2TED@CF$.

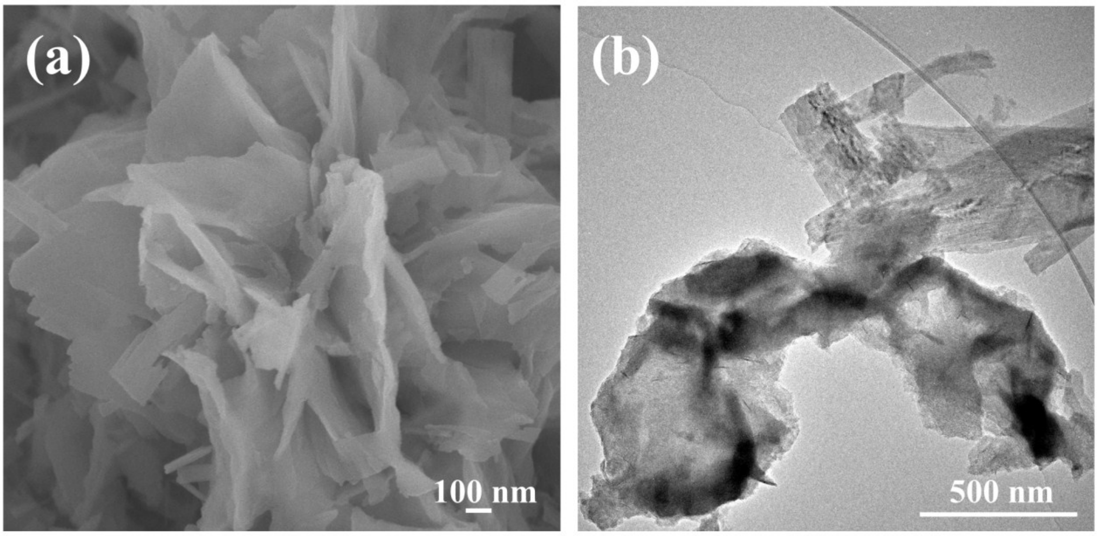

Figure S19. (a) The SEM image of Co/Ni$(BDC)_2$TED@CF after the electrochemical testing and (b) The TEM images of Co/Ni$(BDC)_2$TED@CF after the electrochemical testing.

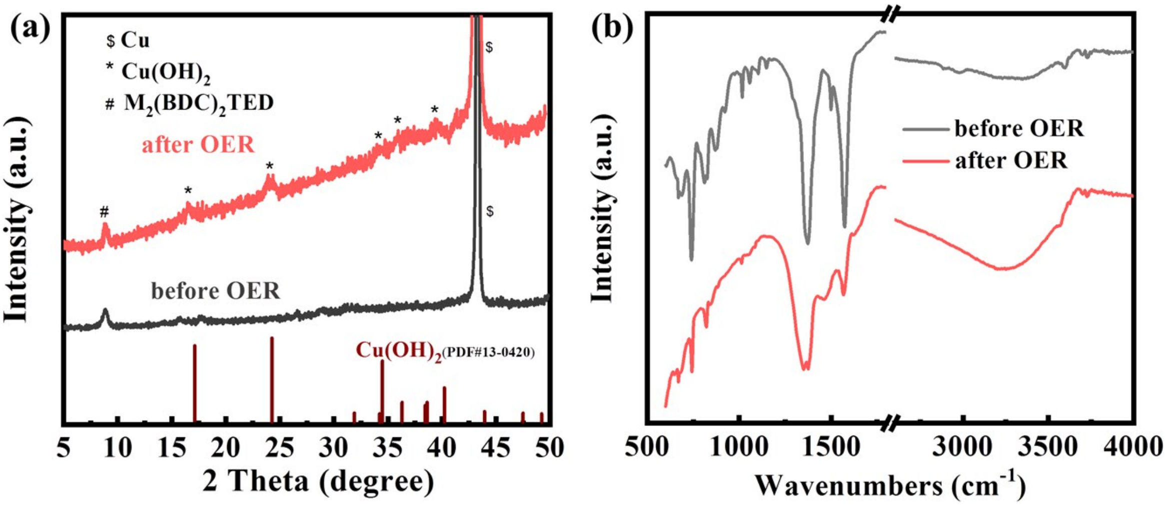

Figure S20. (a) The XRD and (b) IR of Co/Ni$(BDC)_2$TED@CF after the electrochemical testing.

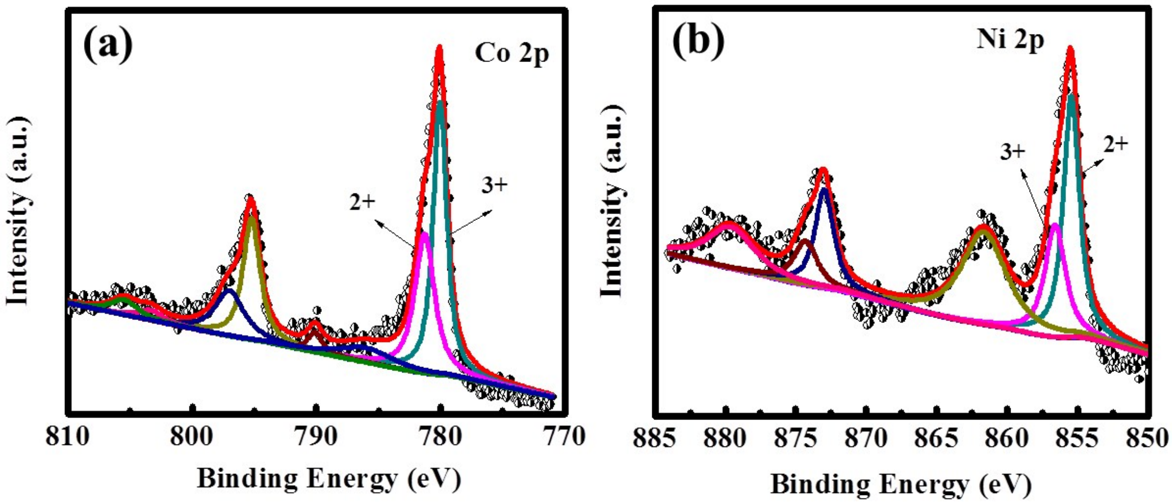

Figure S21. The XPS results of Co/Ni$(BDC)_2$TED@CF after OER test.

Table S1 Comparison of Electrocatalytic Performances of Various Materials

Catalyst	Medium	Overpotential (10 mA/cm^2)	Overpotential (50mA/cm^2)	Tafel slope (mV dec^{-1})	reference
Co/Ni$(BDC)_2$TED@CF nanosheets	1.0 M KOH	260 mV	287 mV	76.24	This work
Ni-MOF@Fe-MOF nanosheets	1.0 M KOH	265 mV	~330 mV	82	[1]
Co-MOF NS/CC	1.0 M KOH	--	370 mV	106.6	[2]
Ti@TiO_2/CdS/ZIF-67	1.0 M NaOH	410 mV	~640 mV	42	[3]
NiFe-UMNs	1.0 M KOH	260 mV	~290 mV	30	[4]
NiFe-MOF array	0.1 M KOH	240 mV	~390 mV	34	[5]
NiCu-MOFNs/NF	1.0 M KOH	--	~280 mV	47.9	[6]

1. K. Rui, G. Zhao, Y. Chen, Y. Lin, Q. Zhou, J. Chen, J. Zhu, W. Sun, W. Huang and S. X. Dou, *Adv. Funct. Mater.*, 2018, **28**, 1801554.
2. Z. Wei, W. Zhu, Y. Li, Y. Ma, J. Wang, N. Hu, Y. Suo and J. Wang, *Inorg. Chem.*, 2018, **57**, 8422-8428.
3. T. Zhang, J. Du, H. Zhang and C. Xu, *Electrochim. Acta*, 2016, **219**, 623-629.
4. G. Hai, X. Jia, K. Zhang, X. Liu, Z. Wu and G. Wang, *Nano Energy*, 2018, **44**, 345-352.

5. J. Duan, S. Chen and C. Zhao, *Nat. Commun.*, 2017, **8**, 15341.

6. X. Zheng, X. Song, X. Wang, Z. Zhang, Z. Sun and Y. Guo, *New J. Chem.*, 2018, **42**, 8346-8350.

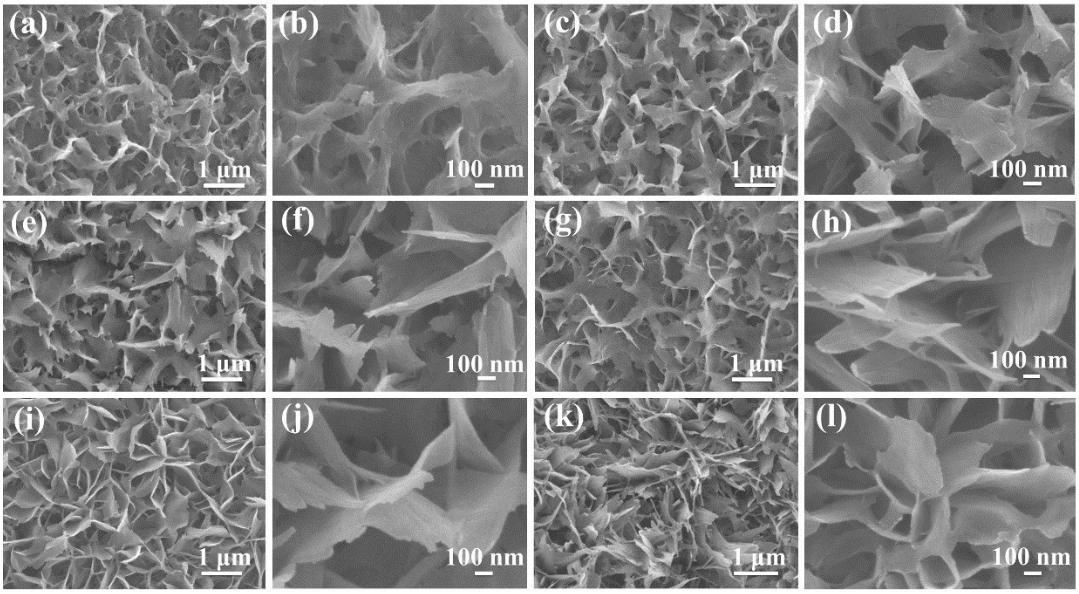

Figure S22. The surface SEM images of Co/Ni$(BDC)_2$TED@CF with different cycles: (a, b) 5 cycles; (c, d) 10 cycles; (e, f) 20 cycles; (g, h) 30 cycles; (i, j) 40 cycles; (k, l) 50 cycles.

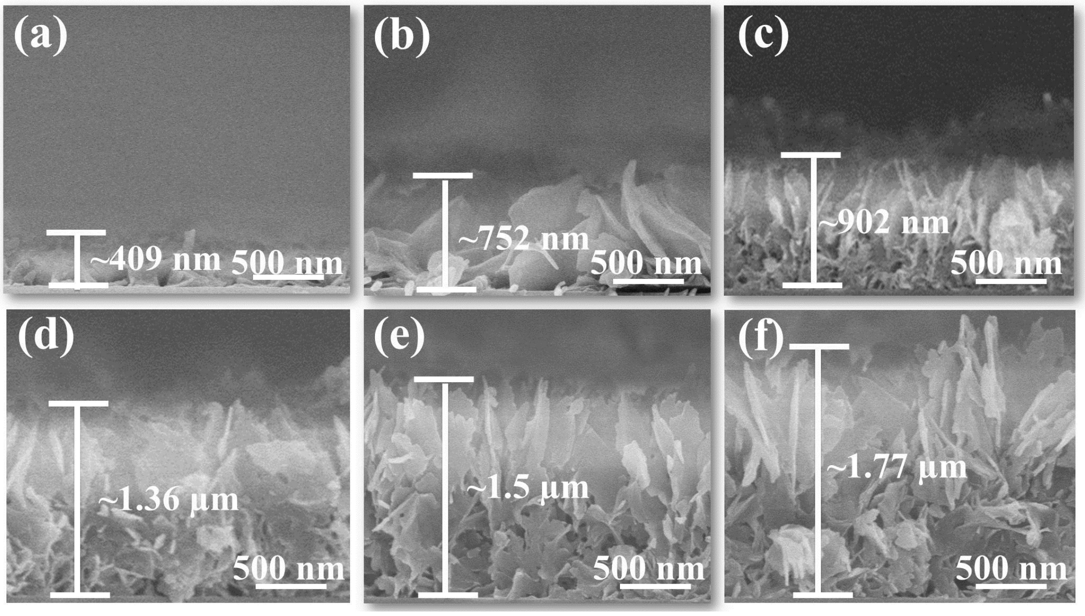

Figure S23. The cross-sectional SEM images of Co/Ni$(BDC)_2$TED@CF with different cycles: (a) (b) 5 cycles; (c) (d) 10 cycles; (e) (f) 20 cycles; (g) (h) 30 cycles; (i) (j) 40 cycles; (k) (l) 50 cycles.

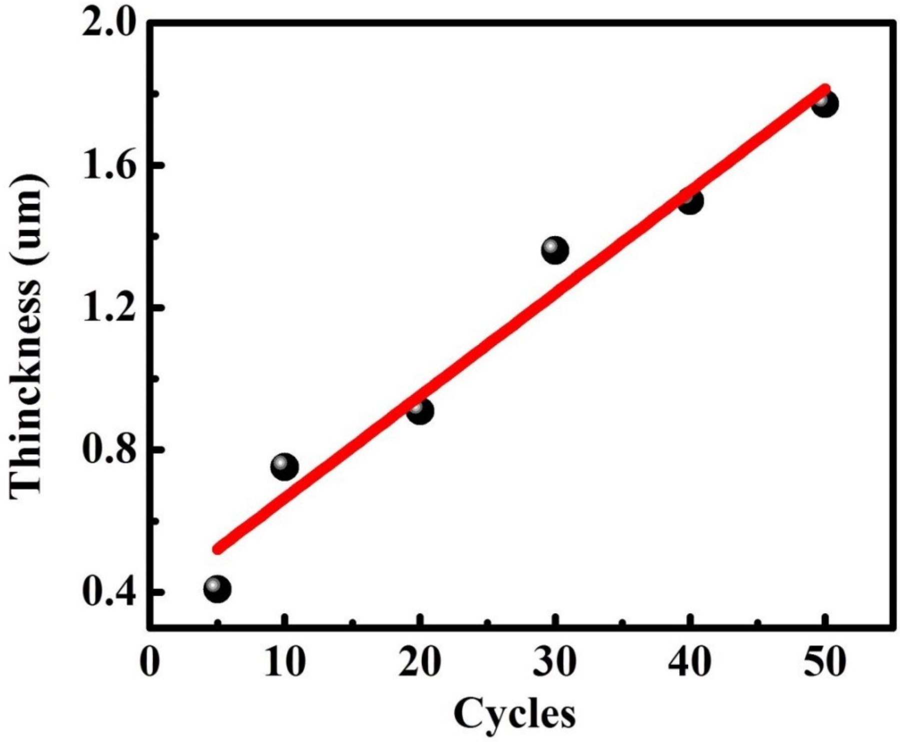

Figure S24. The curves of the thickness versus preparation cycles.

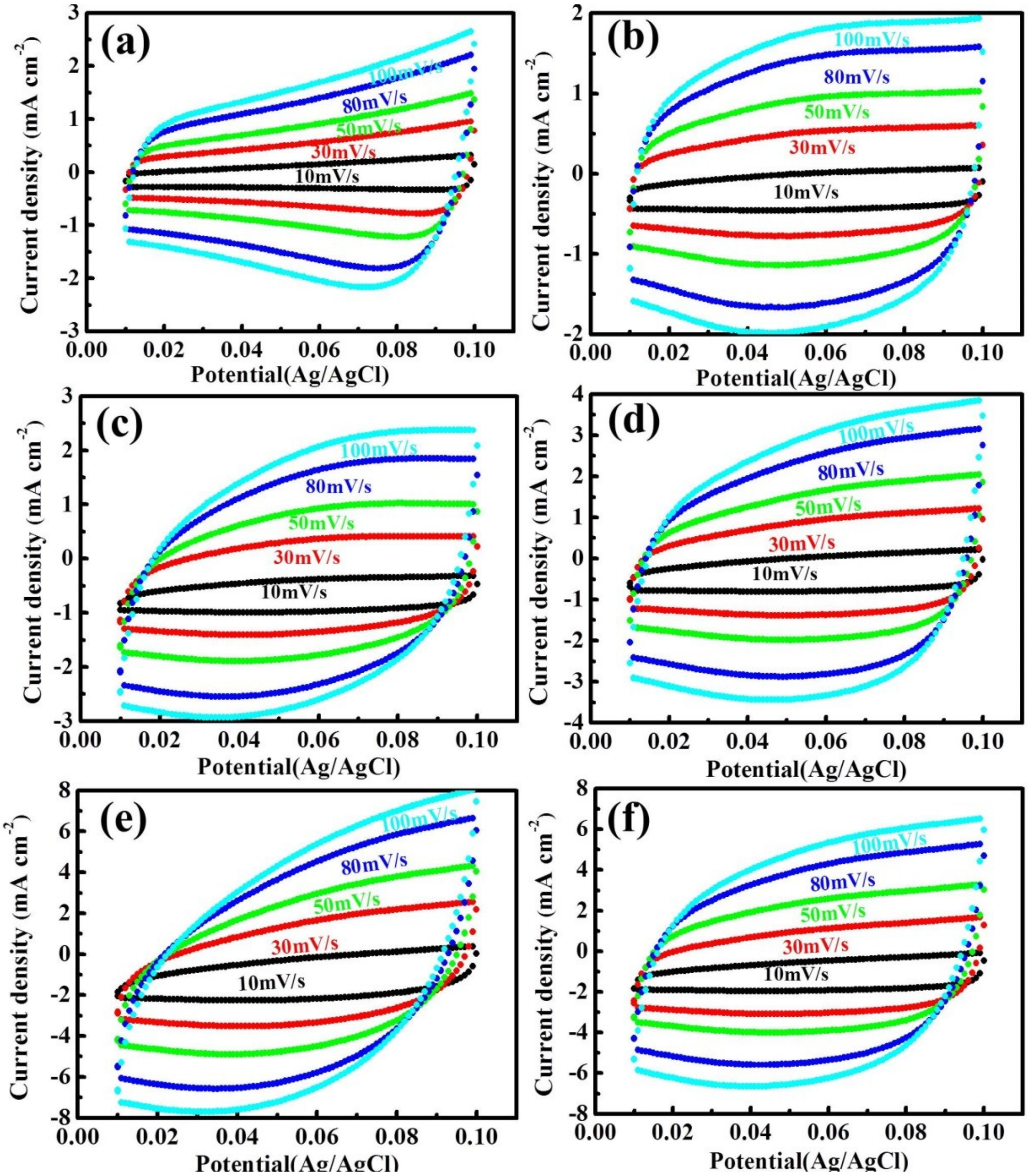

Figure S25. CVs of Co/Ni$(BDC)_2$TED@CF with different thickness at the different scan rates from 10-100 mV s^{-1} in the potential range of 0.01-0.1 V vs Ag/AgCl: (a) 5 cycles; (b) 10 cycles; (c) 20 cycles; (d) 30 cycles; (e) 40 cycles; (f) 50 cycles.

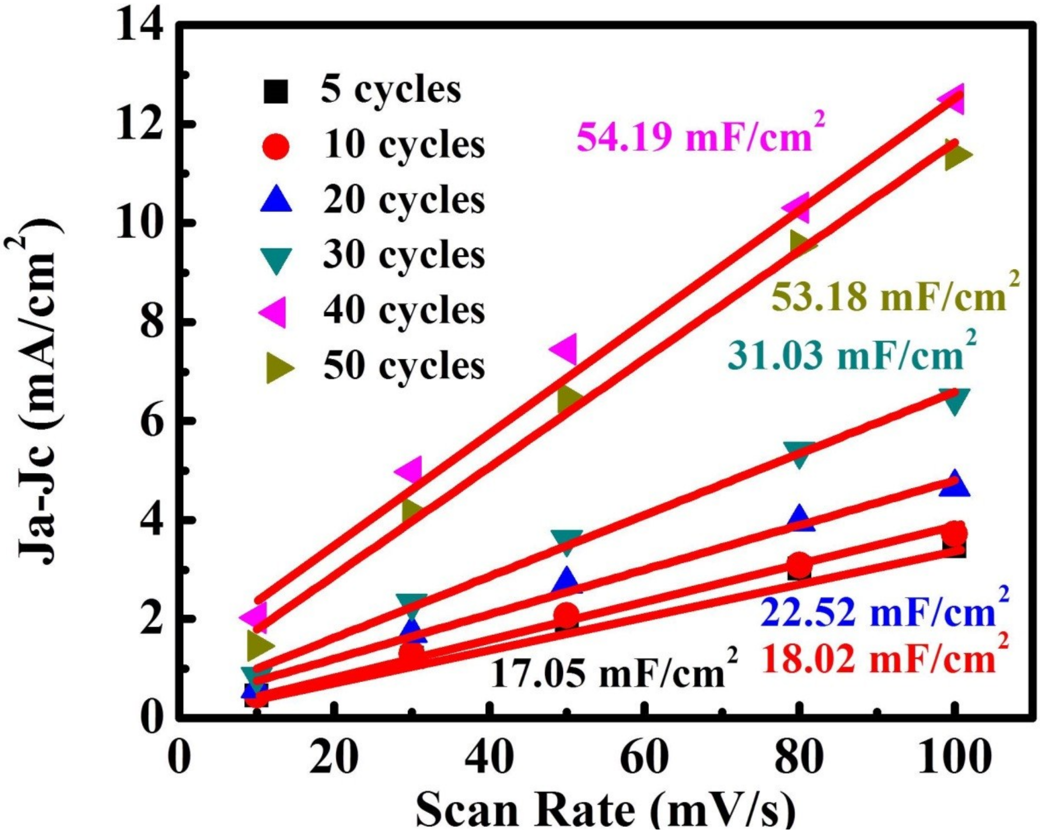

Figure S26. Capacitive current at 0.06 V vs Ag/AgCl for Co/Ni$(BDC)_2$TED@CF with different thickness.

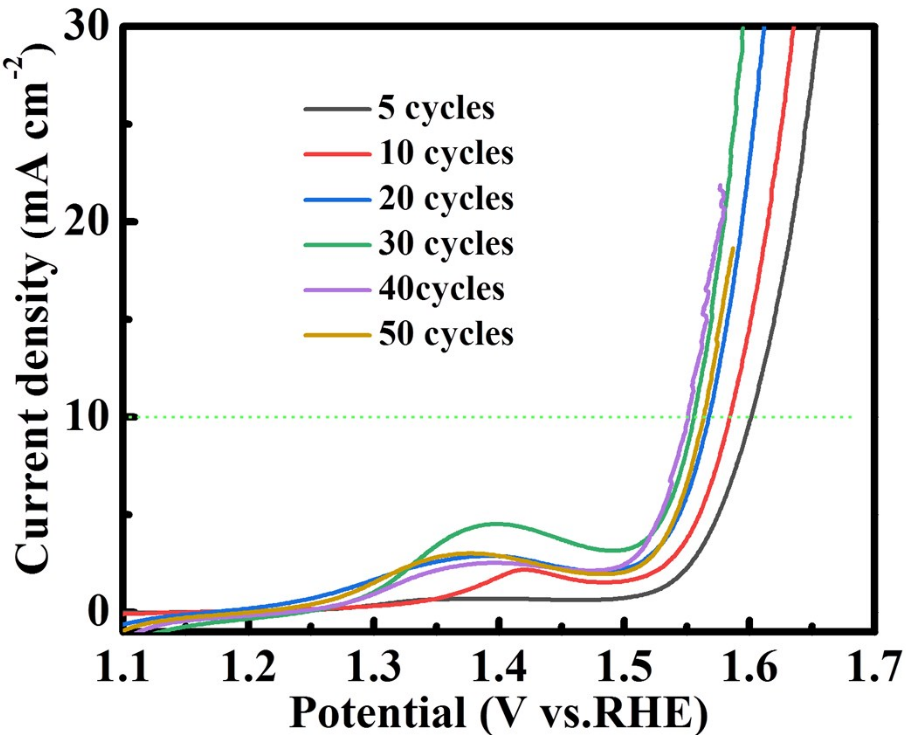

Figure S27. The ECSA normalized LSV curves of Co/Ni$(BDC)_2$TED@CF with different thickness.

element	%
C K	34.44
N K	2.16
O K	36.83
Co K	5.99
Ni K	8.91
Cu K	11.66

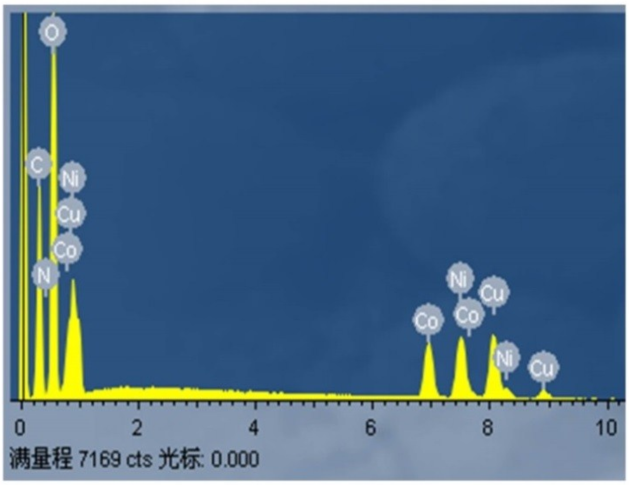

Figure S28. The SEM EDS date of Co/Ni(BDC)$_2$TED@CF with a Co/Ni ratio of 1/1.5 (Cu is from Cu foam).

element	%
C K	37.77
N K	1.87
O K	35.36
Co K	9.06
Ni K	4.54
Cu K	11.40

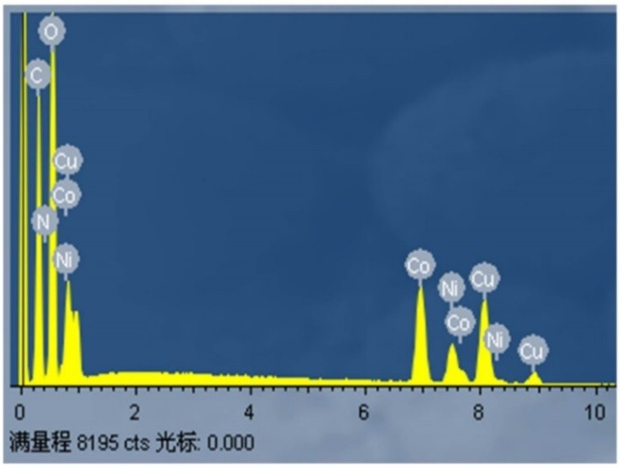

Figure S29. The SEM EDS date of Co/Ni(BDC)$_2$TED@CF with a Co/Ni ratios of 1/0.5 (Cu is from Cu foam).

element	%
C K	41.10
N K	2.77
O K	39.63
Co K	7.76
Ni K	7.12
Cu K	1.61

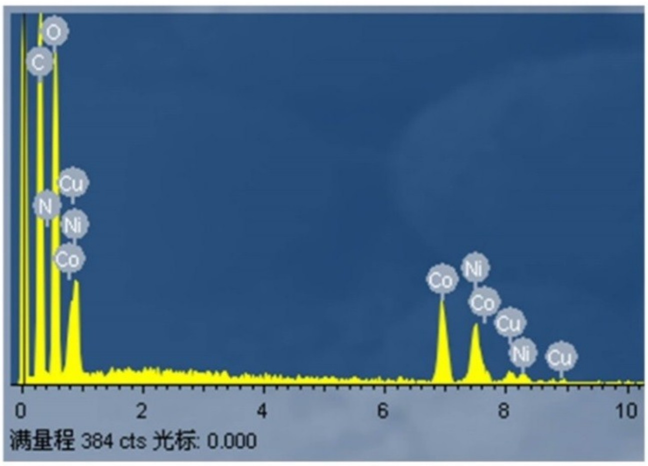

Figure S30. The SEM EDS date of Co/Ni(BDC)$_2$TED@CF with a Co/Ni ratios of 1/1 (Cu is from Cu foam).

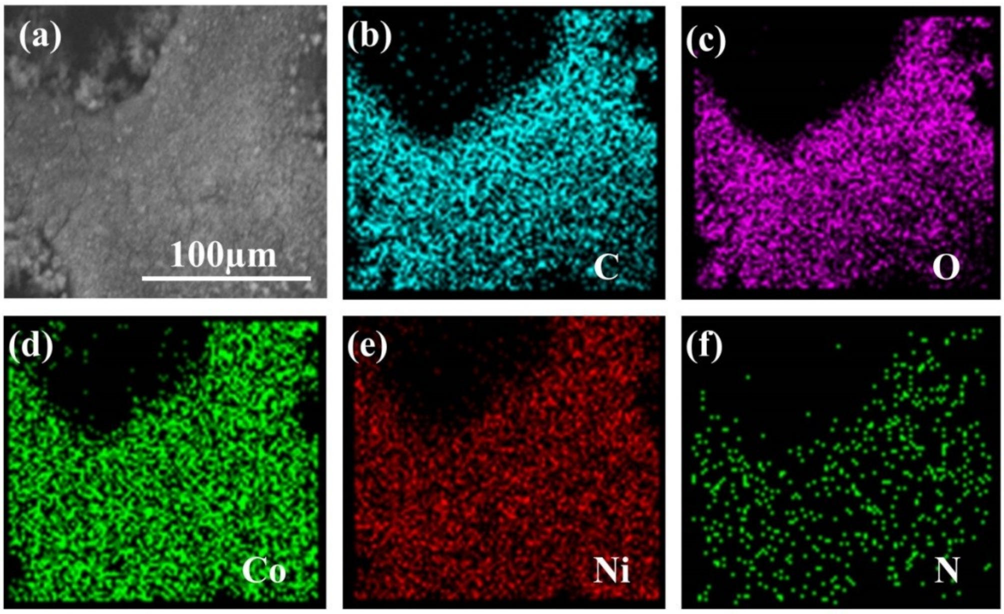

Figure S31. The SEM mapping in Co/Ni$(BDC)_2$TED@CF with a Co/Ni ratios of 1/1.5.

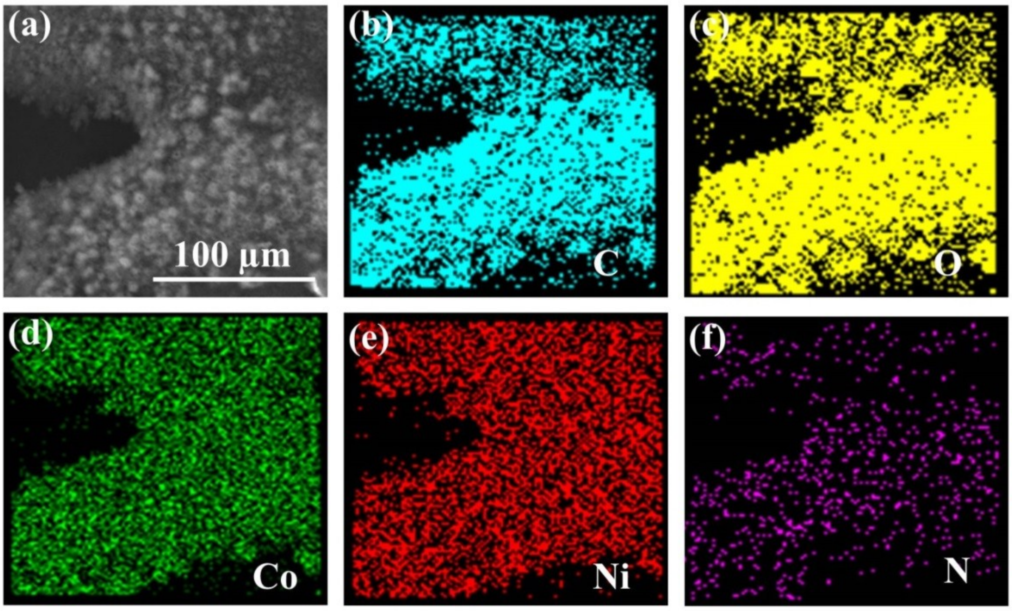

Figure S32. The SEM mapping in Co/Ni$(BDC)_2$TED@CF with a Co/Ni ratios of 1/0.5.

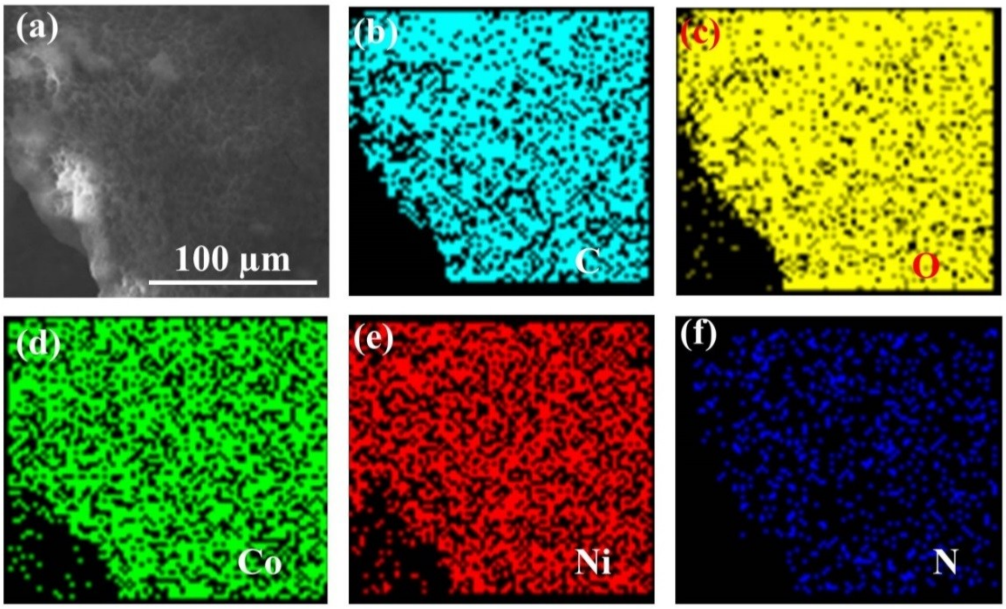

Figure S33. The SEM mapping in Co/Ni$(BDC)_2$TED@CF with a Co/Ni ratios of 1/1.

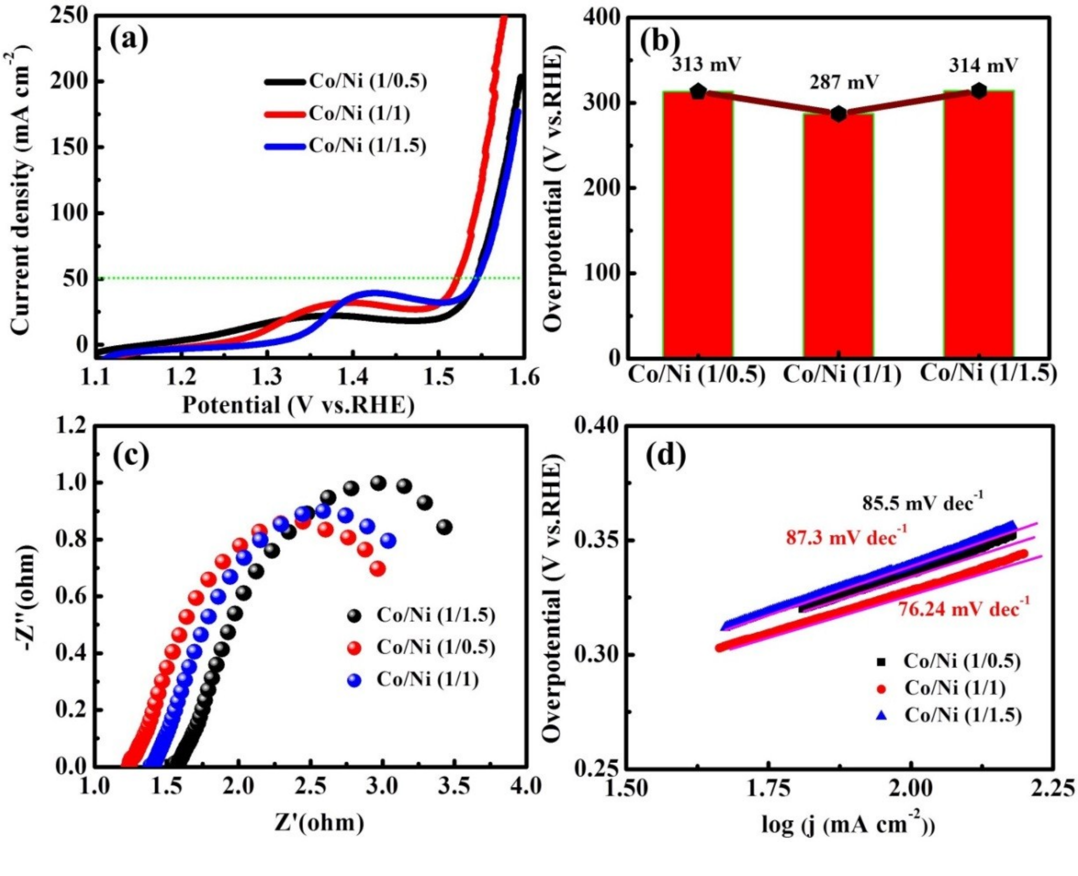

Figure S34. (a) The polarization curves for Co/Ni$(BDC)_2$TED@CF with different Co/Ni ratios; (b) The overpotential of Co/Ni$(BDC)_2$TED@CF with different Co/Ni ratios at the current density of 50 mA/cm^2; (c) The EIS curves; (d) The Tafel plots from the LSV curves.

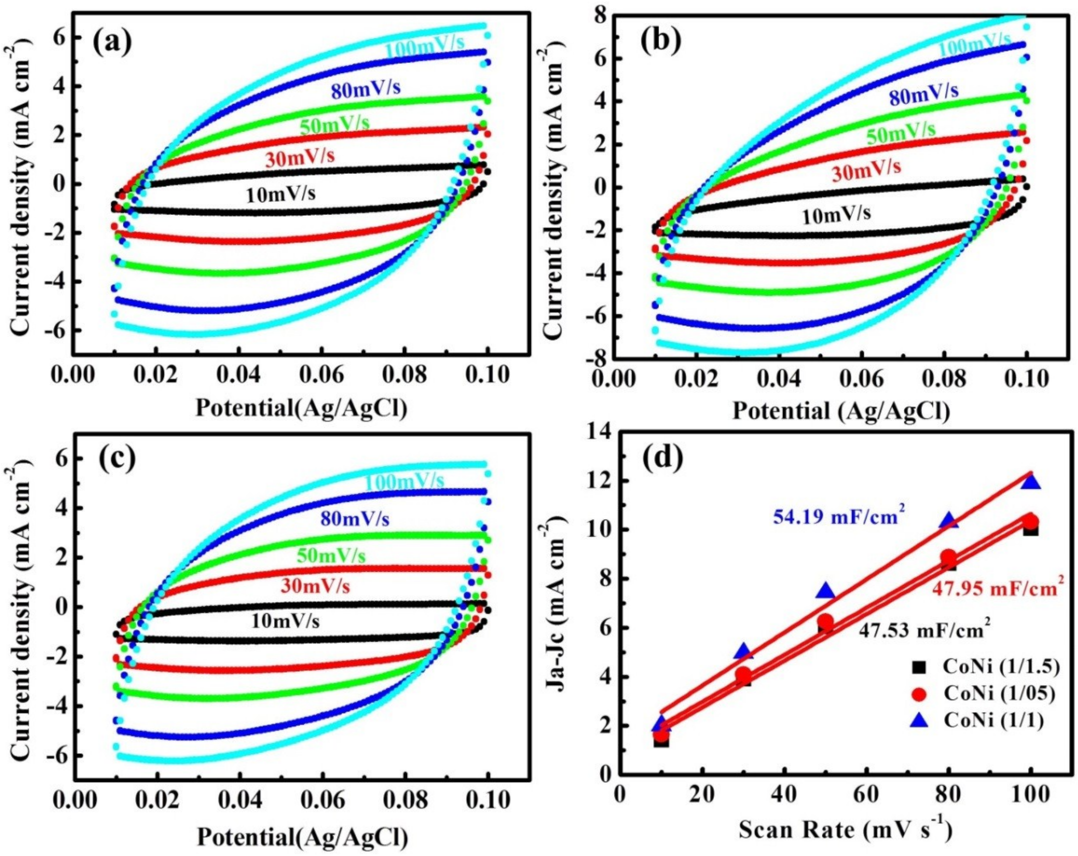

Figure S35. CVs of Co/Ni(BDC)$_2$TED@CF with different Co/Ni ratios at the different scan rates from 10-100 mV s^{-1} in the potential range of 0.01-0.1 V vs Ag/AgCl: (a) Co/Ni(1/05); (b) Co/Ni(1/1); (c) Co/Ni(1/1.5) and (d) Capacitive current at 0.06 V vs Ag/AgCl.

Table S2. The ICP dates of Co/Ni ratios in Co/Ni(BDC)$_2$TED@CF with different Co/Ni ratios.

Sample	concentration	ICP (Co/Ni)	ICP (Co/Ni)	Average Co/Ni ratio
Co/Ni(BDC)$_2$TED@CF(1/1.5)	Co(OAc)$_2$(0.5 mM) Ni(OAc)$_2$(1.0 mM)	17.51/27.3	17.09/25.4	1/1.5
Co/Ni(BDC)$_2$TED@CF(1/0.5)	Co(OAc)$_2$(1.0 mM) Ni(OAc)$_2$(0.5 mM)	19.22/9.81	24.7/11.9	1/0.5
Co/Ni(BDC)$_2$TED@CF(1/1)	Co(OAc)$_2$(1.0 mM) Ni(OAc)$_2$(1.0 mM)	18.17/17.27	18.9/17.7	1/1

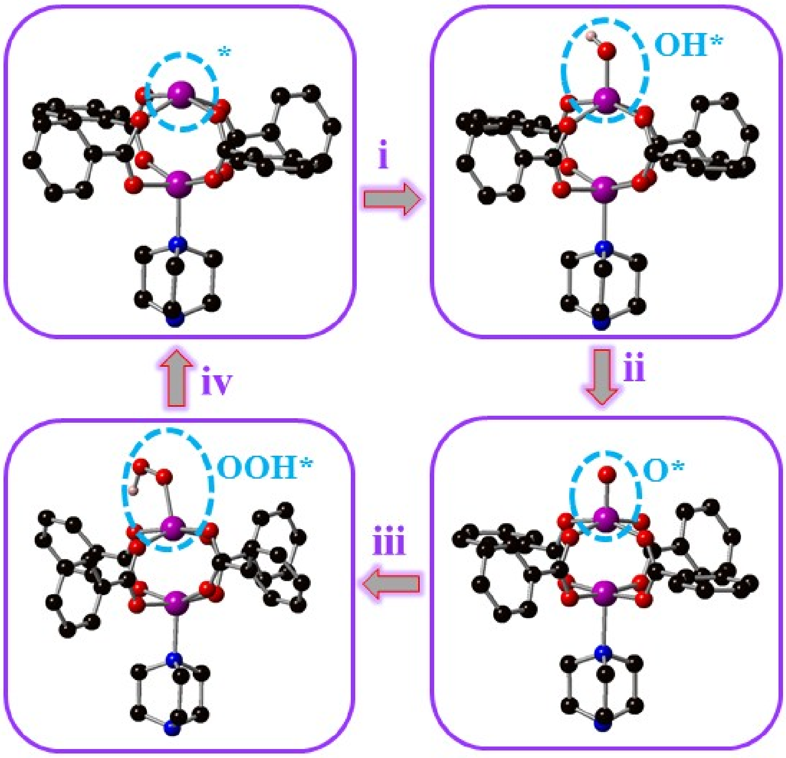

Figure S36. The DFT calculation model of OER process on metal sites in the structure of $Co_2(BDC)_2TED$ with [001] orientation .

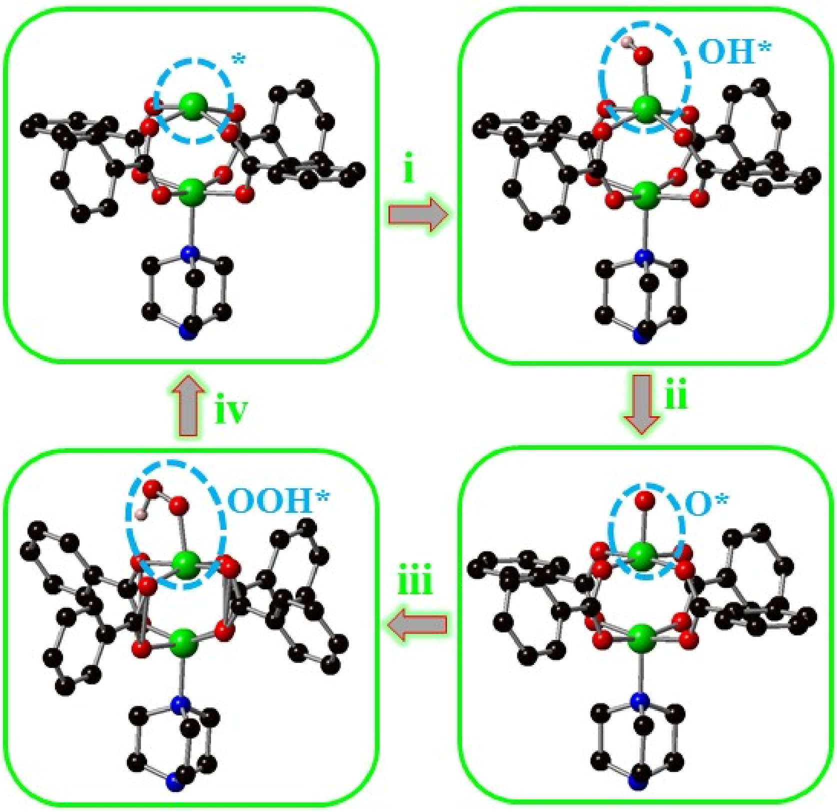

Figure S37. The DFT calculation model of OER process on metal sites in the structure of $Ni_2(BDC)_2TED$ with [001] orientation.

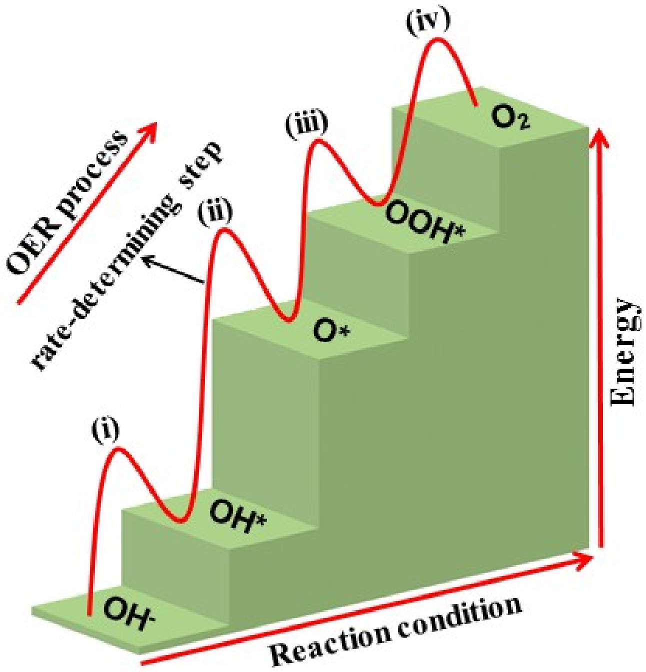

Figure S38. The diagrammatic ghaph of OER process in Co/Ni$(BDC)_2$TED nanosheets.

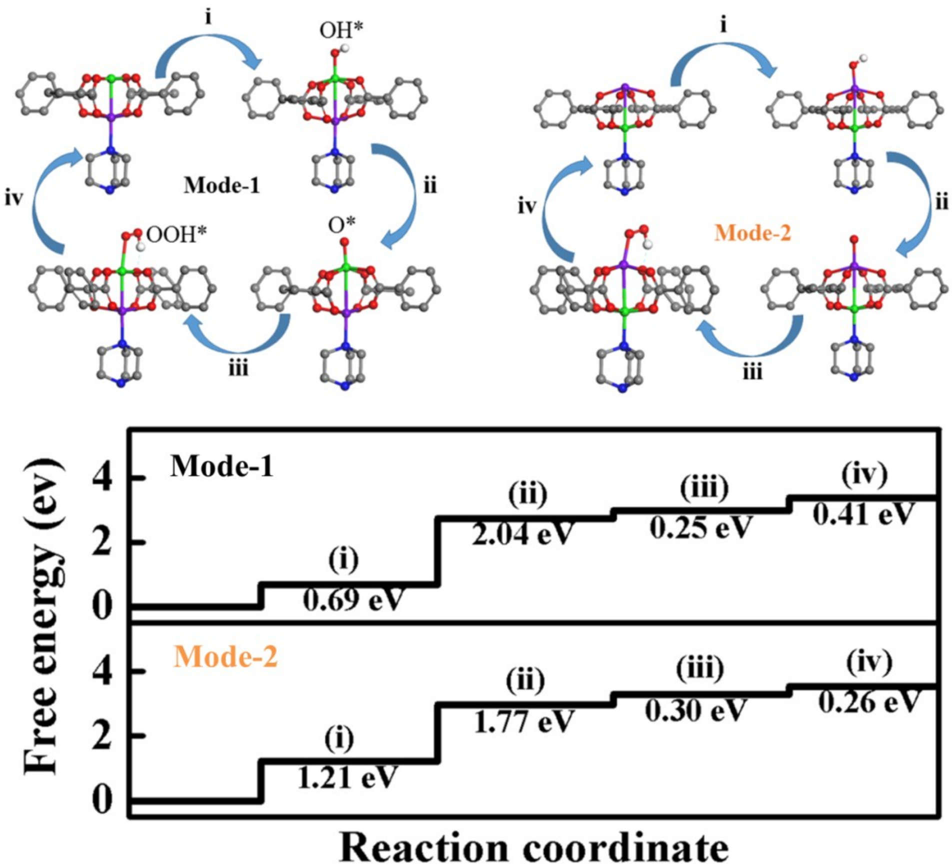

Figure S39. The Gibbs free energy changes of Co/Ni$(BDC)_2$TED nanosheets with two different models.